10-23-2012

Self-Consistent Magnetic Stellar Evolution Models of the Detached, Solar-Type Eclipsing Binary Ef Aquarii

Gregory A. Feiden
Dartmouth College

Brian Chaboyer
Dartmouth College

Follow this and additional works at: https://digitalcommons.dartmouth.edu/facoa

Part of the Astrophysics and Astronomy Commons

arXiv:1210.6177v2 [astro-ph.SR] 13 Nov 2012

SELF-CONSISTENT MAGNETIC STELLAR EVOLUTION MODELS OF THE DETACHED, SOLAR-TYPE ECLIPSING BINARY EF AQUARII

GREGORY A. FEIDEN[1] AND BRIAN CHABOYER

Department of Physics and Astronomy, Dartmouth College, 6127 Wilder Laboratory, Hanover, NH 03755, USA; Gregory.A.Feiden.GR@Dartmouth.edu, Brian.Chaboyer@Dartmouth.edu

Submitted Draft: Version 2; September 24, 2018

ABSTRACT

We introduce a new one-dimensional stellar evolution code, based on the existing Dartmouth code, that self-consistently accounts for the presence of a globally pervasive magnetic field. The methods involved in perturbing the equations of stellar structure, the equation of state, and the mixing-length theory of convection are presented and discussed. As a first test of the code's viability, stellar evolution models are computed for the components of a solar-type, detached eclipsing binary (DEB) system, EF Aquarii, shown to exhibit large disagreements with stellar models. The addition of the magnetic perturbation corrects the radius and effective temperature discrepancies observed in EF Aquarii. Furthermore, the required magnetic field strength at the model photosphere is within a factor of two of the magnetic field strengths estimated from the stellar X-ray luminosities measured by *ROSAT* and those predicted from Ca II K line core emission. These models provide firm evidence that the suppression of thermal convection arising from the presence of a magnetic field is sufficient to significantly alter the structure of solar-type stars, producing noticeably inflated radii and cooler effective temperatures. The inclusion of magnetic effects within a stellar evolution model has a wide range of applications, from DEBs and exoplanet host stars to the donor stars of cataclysmic variables.

Subject headings: binaries: eclipsing — stars: evolution — stars: individual (EF Aquarii) — stars: interiors — stars: low-mass — stars: magnetic field

1. INTRODUCTION

The vast array of physics incorporated in standard low-mass stellar evolution models (see e.g., Chabrier & Baraffe 1997; Baraffe et al. 1998; Dotter et al. 2007, 2008, and references therein) appears to be insufficient for predicting the properties of low-mass stars. Studies of detached eclipsing binary (DEB) systems allow for a very precise determination of the mass and radius of the individual stellar components with uncertainties commonly below 2%. Over the past two decades, these precision studies have accumulated strong evidence that the radii predicted by low-mass stellar evolution models are deflated compared to the observations, at a given mass (e.g., Popper 1997; Torres & Ribas 2002; Ribas 2006; Morales et al. 2009; Torres et al. 2010; Kraus et al. 2011). Typically quoted is that DEB radii appear to be systematically 10% larger than model predictions and DEB effective temperatures are 5% cooler than the models imply. Further evidence has been garnered by studies of single low-mass stars (Berger et al. 2006; Morales et al. 2008), which confirm the aforementioned trends. Although, Boyajian et al. (2012) present results that may be interpreted as counter to these claims.

Recent work has shown that the disagreements may not be as severe as previously believed, when the age and metallicity of the DEBs are considered (Feiden & Chaboyer 2012). Still, many DEB systems display moderately inflated radii (less than 5%) with a small subset displaying radically inflated radii (upward of 10%) compared to stellar models (Feiden & Chaboyer 2012; Terrien et al. 2012). This modest radius offset between observations and models and the presence of strongly inflated stars, suggests that stellar evolution models must invoke new physics to account for the appearance of inflated radii.

Implicated as the culprit for the observed inflated radii and cooler effective temperatures is magnetic activity (Ribas 2006; López-Morales 2007; Morales et al. 2008). The systems at the heart of the problem are often close binaries with short orbital periods. Tidal synchronization of the components acts to spin-up the rotation rate of each star, enhancing the dynamo mechanism and thus supporting a stronger magnetic field within each. While there are a number of direct magnetic field measurements for single stars, there are few among fast rotating binaries. Instead, the hypothesis is reinforced by the presence of strong chromospheric Hα emission (Morales et al. 2008; Stassun et al. 2012), chromospheric Ca II H and K emission (Skumanich et al. 1975), as well as coronal X-ray emission (López-Morales 2007) among inflated stars. The presence of such emission features is considered to be the result of the dissipation of magnetic energy in the stellar atmosphere.

There are, however, stars from DEBs that display inflated radii, despite existing in long-period systems. Both LSPM J1112+7626 (Irwin et al. 2011) and Kepler-16 (Doyle et al. 2011; Winn et al. 2011; Bender et al. 2012) have orbital periods of about 41 days, suggesting that the components are tidally unaffected by the presence of their companion. It is possible that these stars have not had sufficient time to shed angular momentum (Skumanich 1972), preserving strong magnetic fields that they likely possessed near the zero-age main sequence. Whether the low-mass stars in these systems are still magnetically active enough to affect the stellar radius remains unclear. The work by Winn et al. (2011) appears to suggest that Kepler-16 is still relatively young (2 – 4 Gyr) as the primary is more active than the Sun, based on Ca II line emission. This supports the notion that magnetic fields may be influencing the structure of each component. On the other hand, the age of LSPM J1112+7626, estimated from

---

[1] Neukom Graduate Fellow.

gyrochronology, reveals that it is approximately 9 Gyr old (Barnes 2010), supporting the notion that magnetic activity is likely not playing a prominent role in either star's evolution.

Further complicating our picture of low-mass DEBs, KOI-126 (Carter et al. 2011) curiously matches standard stellar evolution models (Feiden et al. 2011; Spada & Demarque 2012). The mass of KOI-126 B and C and their orbital period are very similar to CM Draconis, one of the quintessential low-mass DEB systems displaying inflated radii (Lacy 1977; Morales et al. 2009; Terrien et al. 2012). It is interesting, then, that stellar evolution models would even come close to accurately predicting the observed stellar properties of KOI-126. Given what is known about CM Draconis, one would expect KOI-126 to display inflated radii as a consequence of moderate magnetic activity. Although, MacDonald & Mullan (2012) speculate that KOI-126 should, in fact, not be terribly active and find it unsurprising that standard models should fit the system so well.

Despite the identification of a potential culprit responsible for inflating the radii of DEB components, only ad hoc procedures for treating the effects of magnetic fields have been introduced (Mullan & MacDonald 2001; Chabrier et al. 2007). The method examined by Chabrier et al. (2007) included artificially decreasing the convective mixing-length parameter, so as to mimic the effect of a global magnetic field within the star, as well as artificially reducing the star's bolometric flux in an effort to reproduce the effects of photospheric spots. A second method, proposed by Mullan & MacDonald (2001), altered the Schwarzschild criterion by perturbing the adiabatic gradient in a manner consistent with the work of Gough & Tayler (1966).

Investigations by both groups appear to be at odds with one another. Chabrier et al. (2007) and Morales et al. (2010) claim that starspots appear to be the dominate mechanism inflating stellar radii, and that modifications to convection require unrealistic magnetic field strengths (i.e., reductions in the mixing length in their formulation). On the other hand, Mullan & MacDonald (2001) and MacDonald & Mullan (2012) conclude the opposite that reduction in convective efficiency is ultimately the dominant mechanism. Regardless of which is really the dominant mechanism, both approaches are inherently ad hoc, yet both are capable of reproducing the observed inflated stellar radii.

In this paper, we introduce a self-consistent treatment of a globally pervasive magnetic field embedded in the framework of the Dartmouth stellar evolution code (Dotter et al. 2007, 2008). Our approach follows the outline provided by Lydon & Sofia (1995), though we deviate from their method in a number of ways that are described below. All of the stellar structure equations, including those in the equation of state, are self-consistently modified, as opposed to arbitrarily altering a single quantity. In this way, modifications to the efficiency of thermal convection are accounted for in a more complete fashion, owing to the full thermodynamic treatment of the magnetic field. Overall, the approach used to model magnetic effects can be considered analogous to the parameterized mixing-length treatment of convection.[2] The viability of the models is tested against results from a recent study that characterized the DEB EF Aquarii (Vos et al. 2012).

EF Aquarii (HD 217512; henceforth EF Aqr) is a solar-type DEB found to contain two components displaying drastically

Table 1
Fundamental Stellar Parameters for EF Aqr

Parameter	EF Aqr A	EF Aqr B
$M\,(M_\odot)$	1.244±0.008	0.946±0.006
$R\,(R_\odot)$	1.338±0.012	0.956±0.012
$T_{\rm eff}$ (K)	6150±65	5185±110
[Fe/H]	0.00±0.10	

inflated radii (Vos et al. 2012). Fundamental parameters of the system are quoted in Table 1. What is most striking, is the similarity of the secondary to the Sun and the entire system to α Centauri A and B, in terms of the stellar masses and composition. Although the secondary appears similar to both α Cen B and the Sun, its radius appears to be about 10% larger than one would expect based on stellar evolutionary calculations. The effective temperature of the primary further reveals that both components suffer from substantial radius inflation.

In an effort to reconcile the observations with predictions from theoretical models, Vos et al. (2012) reduced the value of the convective mixing-length. They found $\alpha_{\rm MLT}$ of 1.30 and 1.05 were required for the primary and secondary, respectively, compared to their solar-calibrated value of 1.68. They concluded that fine-tuning the models allows for an accurate description of the observed properties.

Reduction of the required convective mixing length may be physically motivated in two ways: (1) naturally inefficient convection and (2) magnetically suppressed convection. While we must be careful to not read too much into the reality of mixing-length theory, in stellar evolution models the mixing length is an intrinsic "property" of convection. Thus, reducing the mixing length is akin to saying convection is not very efficient at transporting excess energy.

Bonaca et al. (2012) calibrated the convective mixing length for solar-like stars using asteroseismic results provided by the *Kepler Space Telescope*. They found that the value of $\alpha_{\rm MLT}$ in stellar models is tied to stellar properties (i.e., $\log g$, $\log T_{\rm eff}$, and [M/H]). Applying the Bonaca et al. (2012) empirical calibration to the stars in EF Aqr, we find that the primary and secondary component require $\alpha_{\rm MLT} = 1.68$ and 1.44, respectively. Again, compared with their solar calibrated value of $\alpha_{\rm MLT} = 1.68$. The asteroseismically adjusted mixing-lengths are significantly larger than the fine-tuned values determined by Vos et al. (2012). Therefore, it appears that naturally inefficient convection is insufficient to explain the inflated radii of EF Aqr. We are left with the option that magnetic fields may possibly be to blame.

In what is to follow, we describe a self-consistent approach to modeling the effects of a globally pervasive magnetic field with application to the EF Aqr system. Details of the standard Dartmouth models are presented in Section 2 followed by a description of the magnetic perturbations introduced to the code in Sections 3 and 4. Section 5 demonstrates the ability of the invoked perturbations to reconcile the models with the observations. We conclude with a further discussion of the results and their implications in Section 6.

2. MODELS

The framework throughout which magnetic effects are invoked is provided by the Dartmouth Stellar Evolution Program (DSEP; Dotter et al. 2008),[3] a descendant of

---

[2] In so far as reducing an inherently nonlinear, three-dimensional process into terms suitable for a one-dimensional model.

[3] Available at: http://stellar.dartmouth.edu/models/

the Yale Rotating Evolution Code (Guenther et al. 1992). Standard stellar evolution henceforth refers to the basic physics without any magnetic perturbation. The standard physics incorporated in DSEP has been described previously (Chaboyer & Kim 1995; Chaboyer et al. 2001; Bjork & Chaboyer 2006; Dotter et al. 2007, 2008; Feiden et al. 2011), although we will briefly review the elements that are pertinent for the current study.

Above $0.80 M_\odot$, DSEP invokes an ideal gas equation of state (EOS) supplemented by a Debye-Hückel correction in order to account for ion-charge shielding (Chaboyer & Kim 1995). This EOS is computed analytically, in a self-consistent manner, within the code and does not rely on the interpolation within EOS tables. Opacities are drawn from two sources, the OPAL opacities for the high temperature regime (Iglesias & Rogers 1996) complimented by the Ferguson low-temperature opacities (Ferguson et al. 2005). Surface boundary conditions are defined using the PHOENIX AMES-COND model atmospheres (Hauschildt et al. 1999a,b), attached to the model interior where $T = T_{\rm eff}$.

Atomic diffusion and the gravitational settling of helium and heavy elements are implemented using the prescription of Thoul et al. (1994). Additional diffusion effects associated with turbulent mixing (Richard et al. 2005) are also included. Details of the latter are presented in Feiden et al. (2011). Finally, convective core overshoot is treated following the methods outlined by Demarque et al. (2004).

Required before any analysis pertaining to stellar evolution models is calibrating the model properties to the Sun. Determination of the initial solar helium and heavy element mass fractions along with a compatible mixing-length parameter ($Y_{\rm init}$, $Z_{\rm init}$, and $\alpha_{\rm MLT}$, respectively) was performed by calibrating a $1 M_\odot$ model to the Sun. Our solar model was required to reproduce the solar radius, solar luminosity, radius at the base of the convection zone, and the solar photospheric (Z/X) at the solar age (4.57 Gyr; Bahcall et al. 2005). The final set of parameters necessary to satisfy the above criteria for the Grevesse & Sauval (1998) solar composition was $Y_{\rm init} = 0.27491$, $Z_{\rm init} = 0.01884$, and $\alpha_{\rm MLT} = 1.938$.

3. MAGNETIC PERTURBATION

3.1. *Magnetic Field Characterization*

Investigating the effects of a global magnetic field on the interior structure of a star over long time baselines, requires formulating a purely three-dimensional (3D) phenomenon in terms suitable for a one-dimensional (1D) numerical model. Unfortunately, full 3D magnetohydrodynamic (MHD) models are not yet capable of modeling stellar magnetic fields over the long time baselines required for stellar evolutionary calculations. This is in part due to the rapid[4] diffusion of the magnetic field and the immense computational time required. Therefore, in order to probe the effects of a magnetic field, we seek to avoid directly solving the induction equation

$$\frac{\partial \mathbf{B}}{\partial t} = \nabla \times (\mathbf{u} \times \mathbf{B}) + \eta \nabla^2 \mathbf{B}. \tag{1}$$

While not actively seeking a solution to the full suite of 3D MHD equations, it is possible to use the theoretical framework of MHD to provide a reasonably accurate 1D description of a magnetic field and its associated properties. Ultimately, we are able to describe a magnetic field in terms of

the MHD equations and then project out the radial component, the component necessary for stellar evolutionary model computations.

The spatial and temporal evolution of a given magnetic field are governed, quite naturally, by Maxwell's equations,

$$\nabla \cdot \mathbf{E} = 0 \tag{2}$$

$$\nabla \times \mathbf{E} = -\frac{1}{c}\frac{\partial \mathbf{B}}{\partial t} \tag{3}$$

$$\nabla \cdot \mathbf{B} = 0 \tag{4}$$

$$\nabla \times \mathbf{B} = \frac{4\pi}{c}\mathbf{J} \tag{5}$$

where within the stellar plasma, we assume any regions of excess charge inducing an electric potential will rapidly neutralize owing to the mobility of other charges (Debye shielding). Thus, we can safely assume that the plasma is electrically neutral, $\rho_e = 0$. For simplicity, we here made another assumption, that temporal variations of the large-scale field are small, suggesting that the conduction current dominates the displacement current.

Now, let us consider the interactions between the electric and magnetic fields within a dense, ionized fluid moving with arbitrary velocity, $\mathbf{u}$. For slow temporal evolution, non-relativistic dynamics may be described by a single conducting fluid that obeys the classical equations of hydrodynamics coupled with the equations of electromagnetism; the MHD equations (Jackson 1998). Considering a perfectly conducting, non-viscous, non-rotating, compressible fluid in the presence of a gravitational field, the MHD equations governing the system are Ohm's law for a moving fluid,

$$\mathbf{J} = \sigma\left(\mathbf{E} + \frac{\mathbf{u} \times \mathbf{B}}{c}\right), \tag{6}$$

the equation of mass continuity,

$$\frac{\partial \rho_m}{\partial t} + \nabla \cdot (\rho_m \mathbf{u}) = 0, \tag{7}$$

where ρ_m is the mass density, and the fluid equation of motion,

$$\rho_m \frac{d\mathbf{u}}{dt} = \frac{\mathbf{J} \times \mathbf{B}}{c} - \nabla \cdot \overleftrightarrow{\mathbf{P}} + \rho_m \mathbf{g} \tag{8}$$

with $\mathbf{g}$ being the gravitational field vector and $\overleftrightarrow{\mathbf{P}}$ representing the gas pressure tensor. The electromagnetic term in the fluid equation of motion is associated with the assumption that a magnetic field permeates the plasma. However, we have neglected forces associated with any electric fields, for reasons detailed above.

Since, a priori, we have no knowledge of the current density within a given fluid, we replace the current density within Equation (8) using Equation (5). The equation of motion may now be written as

$$\rho_m \frac{d\mathbf{u}}{dt} = \frac{1}{4\pi}(\nabla \times \mathbf{B}) \times \mathbf{B} - \nabla \cdot \overleftrightarrow{\mathbf{P}} + \rho_m \mathbf{g}. \tag{9}$$

With the aid of a vector operation identity and knowing that the magnetic field is divergenceless, this may again be rewritten as

$$\rho_m \frac{d\mathbf{u}}{dt} = \frac{1}{4\pi}(\mathbf{B} \cdot \nabla)\mathbf{B} - \frac{1}{8\pi}\nabla B^2 - \nabla \cdot \overleftrightarrow{\mathbf{P}} + \rho_m \mathbf{g}. \tag{10}$$

Immediately, we recognize that the electromagnetic contributions on the right-hand side are the familiar magnetic tension

---

[4] Relative to a typical stellar lifetime.

and pressure terms, respectively. However, the final form of the equation of motion requires one further step. The first two terms on the right-hand side may be expressed as the divergence of a magnetic stress tensor (Gurnett & Bhattacharjee 2005), let us call it $\overleftrightarrow{\mathbf{T}}$, such that

$$\overleftrightarrow{\mathbf{T}} = -\frac{\mathbf{BB}}{4\pi} + \overleftrightarrow{\mathbf{I}}\frac{B^2}{8\pi} \qquad (11)$$

with $\overleftrightarrow{\mathbf{I}}$ representing the identity tensor. This definition then implies,

$$\rho_m\frac{d\mathbf{u}}{dt} = -\nabla \cdot \left(\overleftrightarrow{\mathbf{T}} + \overleftrightarrow{\mathbf{P}}\right) + \rho_m\mathbf{g}. \qquad (12)$$

The magnetic stress tensor introduced above can be thought of an anisotropic pressure tensor, where the pressures it describes are intrinsic properties of the magnetic field.

Stars, however, are considered to be in hydrostatic equilibrium. This implies the absence of bulk fluid motion, forcing the left-hand side of the equation of motion to vanish. Therefore,

$$\nabla \cdot \left(\overleftrightarrow{\mathbf{T}} + \overleftrightarrow{\mathbf{P}}\right) = \rho_m\mathbf{g}, \qquad (13)$$

which is a statement of magnetohydrostatic equilibrium.

3.2. Stellar Structure Perturbations

At the most fundamental level, one-dimensional stellar evolution codes simultaneously solve a set of four coupled, first-order differential equations.[5] They are the equation of mass conservation, hydrostatic equilibrium, energy transport, and energy conservation. Qualitatively, we can easily predict how these equations will be altered by the presence of a magnetic field which may then be translated into a quantitative description.

The equation of mass conservation should be unaltered by any magnetic perturbation. Of course, this is assuming that mass removed by stellar winds is negligible and that transient events that may remove mass (i.e., flares, coronal mass ejections) are neglected. The stated conditions hold for our approach. Thus,

$$\frac{dr}{dm} = \frac{1}{4\pi r^2\rho} \qquad (14)$$

where we have dropped the subscript m on the density and assume all references to density are specifically to the mass density, unless otherwise noted.

Hydrostatic equilibrium, as we saw earlier in Equation (13), is modified through the inclusion of the magnetic pressure and tension. Projecting out the radial component of the magnetic pressures, we are able to adapt the three-dimensional concept for one-dimensional models. Therefore, we have

$$\frac{dP}{dm} = -\frac{Gm}{4\pi r^4} + \frac{1}{4\pi r^2\rho}\left[\frac{(\mathbf{B}\cdot\nabla)\mathbf{B}}{4\pi} - \nabla\left(\frac{B^2}{8\pi}\right)\right] \cdot \hat{\mathbf{r}}. \qquad (15)$$

The precise handling of the vector magnetic field within the code will be discussed later.

The final form of the energy transport equation is the same as if there were no perturbation. Namely,

$$\frac{dT}{dm} = \frac{T}{P}\nabla_{\text{temp}}\frac{dP}{dm} \qquad (16)$$

[5] There are additional equations often included to account for atomic diffusion. While included in DSEP, we do not seek perturbations to these equations at the present time. See Mathis & Zahn (2005) for a rigorous treatment of mixing associated with magnetic fields.

where ∇_{temp} is the local temperature gradient. Magnetic perturbations to the stellar structure equations will self-consistently alter the temperature gradient through various thermodynamic considerations. Of greatest importance will be the affects on the treatment of convection. The full treatment will be discussed in the next subsection.

Finally, there are changes to the parameters present in the canonical equation of energy conservation in stellar evolution. Modifications to these parameters arise from the treatment of the specific thermodynamic equations (discussed in the next subsection) and additional terms that are electromagnetic in origin. The final form of the energy conservation equation is

$$\frac{dL}{dm} = \varepsilon - \frac{dU}{dt} + \frac{P}{\rho^2}\frac{d\rho}{dt} + \frac{Q_{\text{ohm}}}{\rho} + \frac{F_{\text{Poynt}}}{\rho}. \qquad (17)$$

Aside from the first three standard terms on the right-hand side, there are two additional electromagnetic terms. First, there is a Poynting flux associated with the field,

$$F_{\text{Poynt}} = \frac{c}{4\pi}\mathbf{E} \times \mathbf{B}, \qquad (18)$$

although as discussed above, we assume the E-field is zero everywhere. Next, energy is also associated with the Ohmic dissipation of electric currents brought about by the resistive nature of the plasma.

$$Q_{\text{ohm}} \propto I^2R, \qquad (19)$$

where I is the electric current and R is the resistance of the medium. Here, electrical currents are converted to heat that then is transmitted to the surrounding plasma. Since we have assumed an infinitely conducting plasma, this energy term goes immediately to zero.

3.3. Thermodynamic Considerations

The effects of a global magnetic field are introduced into the thermodynamic framework supplied by DSEP following the approach outlined by Lydon & Sofia (1995, hereafter LS95). Providing a detailed, step-by-step guide of the magnetic perturbation to the various thermodynamic quantities would prove tedious. Therefore, we refer the reader to LS95 for a full derivation of each equation presented below. Our aim in this subsection is to adequately summarize the pertinent aspects of LS95 and highlight where we diverge from their original approach.

At the core of the LS95 method is the specification of a new thermodynamic state variable, χ, such that

$$\chi = \chi(r, \rho) = \frac{U_\chi}{\rho} = \frac{B(r)^2}{8\pi\rho}. \qquad (20)$$

The state variable χ is the magnetic energy per unit mass and $B(r)$ is the magnetic field strength at radius r. Unlike LS95, our definition of χ depends on the radial distribution of the magnetic field strength and also on the density of the stellar plasma. Originally, LS95 favored a mass-depth-dependent function, $\chi(M_r)$. However, we moved away from this prescription when we realized several thermodynamic derivatives became divergent. Once the magnetic field strength is specified throughout the star, it is straightforward to calculate χ at each point within the model.

The energy associated with the magnetic field arises due to forces exerted by the magnetic field on the plasma. These forces are represented by the anisotropic pressure tensor

present in Equation (12). As a first approximation, we convert the pressure tensor to a scalar pressure by taking the trace of the pressure tensor to yield the mean magnetic pressure,

$$\langle P_{\mathrm{mag}}\rangle \sim \frac{1}{3}\mathrm{Tr}\left(-\frac{\mathbf{BB}}{4\pi} + \overleftrightarrow{\mathbf{I}}\frac{B^2}{8\pi}\right). \tag{21}$$

Since we are not solving the full set of MHD equations, we look, instead, to set approximate upper and lower limits on the scalar pressure. Assuming a Cartesian coordinate system, if we imagine the magnetic field is parallel to the z-axis, or for a star, the rotational axis, then we may expand the pressure tensor to read

$$\overleftrightarrow{\mathbf{T}} = \begin{bmatrix} B^2/8\pi & 0 & 0 \\ 0 & B^2/8\pi & 0 \\ 0 & 0 & -B^2/4\pi + B^2/8\pi \end{bmatrix}. \tag{22}$$

Note that there is an isotropic magnetic pressure associated with each diagonal element along with the additional magnetic tension term in the final element. Since tension is directed along the field line, the tension exists in the z-direction only, in this instance. Taking the trace, we find

$$\langle P_{\mathrm{mag}}\rangle = \frac{1}{3}\left(\frac{B^2}{8\pi}\right) = \frac{1}{3}\chi\rho. \tag{23}$$

The above equation is satisfied for a magnetic field where a strong tension component is present. However, if we assume that there is no tension at all, then, following the same procedure,

$$\langle P_{\mathrm{mag}}\rangle = \frac{1}{3}\left(\frac{3B^2}{8\pi}\right) = \chi\rho. \tag{24}$$

We can now limit the strength of the scalar magnetic pressure within the one-dimensional framework. Specifically,

$$\frac{1}{3}\chi\rho \leq \langle P_{\mathrm{mag}}\rangle \leq \chi\rho. \tag{25}$$

Defining a "geometry parameter," akin to LS95, allows us to emulate the effects of having a strongly curved field or a field with no curvature, and varying degrees between the two extremes. This geometry parameter is defined such that we recover the average magnetic pressure for each case above,

$$\langle P_{\mathrm{mag}}\rangle = (\gamma - 1)\chi\rho \equiv P_\chi \tag{26}$$

where

$$\gamma = \begin{cases} 2 & \text{tension-free} \\ 4/3 & \text{maximum tension} \end{cases}. \tag{27}$$

In both cases, the appropriate expression for the scalar magnetic pressure is returned. With the magnetic energy density and pressure formulated as scalars, we have successfully converted the inherently three-dimensional magnetic field into a one-dimensional magnetic perturbation. In the process, we have also reproduced the scalar parameters originally presented by LS95.

3.3.1. *Equation of State*

The derivations that follow hereafter in Sections 3.3.1 and 3.3.2 are provided as a review of the LS95 method to enable transparency and enhance the clarity of discussions concerning the application of our models. Original, complete derivations are to be found in LS95. We do, however, deviate from

their paper in Equation (65), where it is stated explicitly below.

We have just seen that magnetic fields exert forces on the plasma and, thus, carry an associated pressure, tension, and energy. The introduction of these terms into the equations of stellar structure then necessitates the inclusion of these parameters in the EOS of the system. Again, we will mention only the most important modifications, deferring to LS95 for a rigorous treatment. Beginning with the first law of thermodynamics,

$$dQ = TdS = dU + PdV \tag{28}$$

we recognize that each term contains, now, both the standard gas and radiation terms as well as a new magnetic contribution,

$$dQ = T(dS_0 + dS_\chi) = (dU_0 + dU_\chi) + P_0 dV. \tag{29}$$

In the above equation, the magnetic perturbation rightly does not contribute any work. However, in order to write the equation as a function of the total pressure, we may subtract off the magnetic contribution,

$$TdS = dU + PdV - (\gamma - 1)\frac{\chi}{V}dV \tag{30}$$

where we take the volume to be the specific volume, $V = \rho^{-1}$. Hereafter, it is also assumed that any unsubscripted quantity refers to the total quantity while gas and radiation are lumped under the subscript 0 (zero) convention and magnetic variables carry a subscript χ.

Equation (30) is the new "non-standard" first law of thermodynamics and suggests that

$$V \text{ or } \rho = f(P, T, \chi)$$

and

$$U \text{ or } S = f(\rho, T, \chi).$$

Following the derivation by LS95, explicitly writing out the other state variables illustrates the effects of adding the magnetic perturbation. Ignoring constants for clarity and ease,

$$P = \rho T + \frac{1}{3}T^4 + \chi\rho(\gamma - 1) \tag{31}$$

$$\rho = \left[P - T^4/3\right] / \left[T + (\gamma - 1)\chi\right] \tag{32}$$

$$U = \frac{3}{2}T + \frac{T^4}{\rho} + \chi \tag{33}$$

which are all subject to the EOS,

$$\frac{d\rho}{\rho} = \alpha\frac{dP}{P} - \delta\frac{dT}{T} - \nu\frac{d\chi}{\chi}. \tag{34}$$

The coefficients in the EOS above are defined as follows,

$$\alpha = \left(\frac{\partial \ln\rho}{\partial \ln P}\right)_{T,\chi} \tag{35}$$

$$\delta = -\left(\frac{\partial \ln\rho}{\partial \ln T}\right)_{P,\chi} \tag{36}$$

$$\nu = -\left(\frac{\partial \ln\rho}{\partial \ln\chi}\right)_{P,T} \tag{37}$$

and will be referred to, as such, throughout the rest of the paper. Note, that α carries no subscript and should not be confused with the convective mixing-length parameter, α_{MLT}.

An immediate consequence of altering the thermodynamic variables is the effect on the specific heats,

$$c_P = \left(\frac{dQ}{dT}\right)_{P,\chi} = \left(\frac{dU}{dT}\right)_{P,\chi} + [P - (\gamma-1)\chi\rho]\left(\frac{dV}{dT}\right)_{P,\chi} \quad (38)$$

$$c_V = \left(\frac{dQ}{dT}\right)_{V,\chi} = \left(\frac{dU}{dT}\right)_{V,\chi} \quad (39)$$

which are related to one another via the relation,

$$c_P - c_V = \frac{P\delta^2}{\rho T\alpha}. \quad (40)$$

The difference in specific heats is written just as it would be without any magnetic perturbation, however, each term is self-consistently modified by the presence of a magnetic perturbation.

The change in heat as a result of the magnetic perturbation follows and is found to be

$$dQ = c_P dT - \frac{\delta}{\rho}dP + \left(\frac{P\delta\nu}{\rho\alpha\chi} + 1\right)d\chi, \quad (41)$$

although, the addition of the purely magnetic term, $d\chi$, as a result of the perturbation should not be included. The reasoning for this is simple. If we assume that magnetic phenomena are generated through the dynamo action, then we inference that rotational energy is the source for the energy converted to the pure magnetic term. Since our models do not account for rotation, we discard the final term in the above equation. Thus, the change in heat to be considered in the stellar luminosity equation is

$$dQ = c_P dT - \frac{\delta}{\rho}dP + \frac{P\delta\nu}{\rho\alpha\chi}d\chi. \quad (42)$$

LS95 were quick to point out, that at the instant of any magnetic perturbation, the change in heat due to magnetic effects should be exactly zero.

Finally, from the observed change in heat comes the definition of the adiabatic gradient. Adiabaticity requires constant entropy, and therefore no heat exchange, meaning

$$\nabla_{ad} = \left(\frac{d\ln T}{d\ln P}\right)_{S,\chi} = \frac{P\delta}{\rho T c_P} \quad (43)$$

as it is in the non-magnetic case. Again, only in appearance; the actual variables are altered by the introduction of a magnetic perturbation.

3.3.2. *Mixing-length Theory*

Convection is determined to occur in regions where a given fluid parcel is unstable to a small displacement in the radial direction. The primary method of determining convective stability is to analyze the density of a generalized fluid parcel. Parcels that are less dense than their surroundings will travel radially outward until they reach a height within the star at which the surrounding fluid has the same density as the parcel.

Upon reaching this point, the fluid parcel is assumed to fully mix with its surroundings becoming indistinguishable from the rest of the fluid. Conversely, if a fluid element is more dense than surrounding fluid, it will sink down to a greater depth in the star, following the same trend as a rising convective element. In either case, gravity is the restoring force. One

assumption is that the fluid parcel is considered to always be in pressure equilibrium with its surroundings.

The distance over which a fluid parcel travels before mixing is the well-known "mixing-length." Mixing-length theory (MLT) has been well established as a local means of prescribing convection for a one-dimensional stellar evolution code (Vitense 1953; Böhm-Vitense 1958). At locations where various differences in prescriptions of MLT occur, we will specify our assumptions.

Stability of a fluid parcel is determined by comparing the density of the element to that of the surroundings

$$D\rho = \left[\left(\frac{d\rho}{dr}\right)_e - \left(\frac{d\rho}{dr}\right)_s\right]\Delta r \quad (44)$$

where e and s denote quantities of the fluid element under consideration and the surroundings, respectively. To ensure stability, we require $D\rho > 0$, meaning, the element is stable to small radial displacements,

$$\left(\frac{d\rho}{dr}\right)_e - \left(\frac{d\rho}{dr}\right)_s > 0. \quad (45)$$

As the fluid parcel is displaced radially, LS95 reminds us that we must consider how χ of the parcel reacts. If the initial χ of the parcel does not change as the element is displaced,

$$\left(\frac{d\ln\chi}{dr}\right)_e = 0.$$

Conversely, if χ of the element is always equal to that of the surrounding material, there must be a flux of χ as the element is displaced,

$$\left(\frac{d\ln\chi}{dr}\right)_e = \left(\frac{d\ln\chi}{dr}\right)_s.$$

It is therefore advantageous to relate the spatial gradient of magnetic energy density of the parcel to that of the surroundings by introducing a free parameter, f, such that

$$\left(\frac{d\ln\chi}{dr}\right)_e = f\left(\frac{d\ln\chi}{dr}\right)_s \quad (46)$$

where f varies between 0 and 1. Later, we will attempt to eliminate this free variable and set it to a physically realistic value.

Expanding the density differentials introduced in Equation (45) and multiplying through by the pressure scale height[6] casts the stability criterion according to known differentials,

$$\delta\nabla_e - (1-f)\nu\nabla_\chi - \delta\nabla_{temp} > 0. \quad (47)$$

where we made use of a series gradient definitions,

$$\nabla_{temp} \equiv \left(\frac{d\ln T}{d\ln P}\right)_s \quad (48)$$

$$\nabla_e \equiv \left(\frac{d\ln T}{d\ln P}\right)_e \quad (49)$$

$$\nabla_\chi \equiv \left(\frac{d\ln\chi}{d\ln P}\right)_s = \left(\frac{d\ln\chi}{dr}\right)_s\left(\frac{dr}{d\ln P}\right)_s. \quad (50)$$

[6] Here, we reveal that we are basing our MLT formulation on the pressure scale height, $H_P = -(dr/d\ln P)$, as opposed to the temperature scale height since we assume pressure equilibrium between the fluid parcel and its surroundings.

Here, we have defined the temperature gradient of the surrounding plasma, temperature gradient fluid element in question, and the magnetic energy density gradient, respectively.

The magnetic energy density gradient turns out to affect the final form of the temperature gradient of the fluid parcel. In particular, the relation between the gradient of the parcel and that of the surrounding fluid, given by Equation (46). If $f = 0$, then we find that complete adiabaticity holds, meaning $\nabla_e \rightarrow \nabla_{ad}$. However, for the case that $f \neq 0$, any heat transferred away from the parcel will be in the form of magnetic energy ($dQ = d\chi$). Thus, from Equation (42),

$$0 = c_P dT_e - \frac{\delta}{\rho} dP_e + \frac{P\delta v}{\rho\alpha\chi} d\chi_e \tag{51}$$

which may be rearranged to read

$$\nabla_e = \nabla_{ad} - f\frac{v}{\alpha}\nabla_{ad}\nabla_\chi. \tag{52}$$

Substituting this expression for the parcel's temperature gradient back into Equation (47), we derive the condition that must be met if a fluid parcel is to be stable against convection,

$$\nabla_{ad} - f\frac{v}{\alpha}\nabla_{ad}\nabla_\chi - (1-f)\frac{v}{\delta}\nabla_\chi > \nabla_{temp}. \tag{53}$$

With a modified stability criterion in hand, LS95 the proceed to derive a set of five equations that allow for a solution to the temperature gradient, ∇_{temp}. The equations are developed through a detailed consideration of the various energy fluxes through the system in their Sections 5.1 – 5.3. The final five equations comprising their magnetic mixing-length description of convection are

$$F_{tot} = \frac{4acG}{3} \frac{T^4 M_r}{\kappa P r^2} \nabla_{rad} \tag{54}$$

$$F_{tot} = \frac{4acG}{3} \frac{T^4 M_r}{\kappa P r^2} \nabla_{temp} + F_{conv} \tag{55}$$

$$F_{conv} = \rho v_{conv} \left[c_P DT + \frac{P\delta v}{\rho\alpha\chi} D\chi \right] \tag{56}$$

$$v_{conv}^2 = \frac{g\ell_m^2 \delta}{8H_P} \left[(\nabla_{temp} - \nabla_e) + \frac{v}{\delta}(1-f)\nabla_\chi \right] \tag{57}$$

$$\frac{2acT^3}{\rho v_{conv} c_P} \left[\frac{\omega}{1 + \ddot{y}\omega^2} \right] (\nabla_{temp} - \nabla_e)$$
$$= (\nabla_e - \nabla_{ad}) + f\frac{v}{\alpha}\nabla_{ad}\nabla_\chi \tag{58}$$

where we must now take a moment to dissect the various pieces.

The first two equations above describe the total flux if only radiation is carrying energy and in the case that convection is also present, respectively. Within those two equations, a, c, and G are, respectively, the radiation constant, speed of light in a vacuum, and the gravitational constant. M_r is the mass contained within a spherical volume characterized by the radius, r, and κ is the radiative opacity. Lastly, ∇_{rad} is the radiative temperature gradient.

Equation (56) is the energy flux transported by convection. The quantities, DT and $D\chi$ are defined the same as $D\rho$ in Equation (45). Another variable, the convective velocity v_{conv} is also introduced and characterizes the velocity of the fluid within a convection cell.

The convective velocity is then defined in Equation (57) and contains a single parameter not previously mentioned, ℓ_m. This parameter is the convective mixing-length, ℓ_m, which is further defined as some multiple of the pressure scale height (i.e., $\ell_m = \alpha_{MLT} H_P$). Note that the mixing-length introduces the canonical convective mixing-length parameter, α_{MLT}, into the discussion.

Last of the five equations of MLT describes how the convective gradient is connected to the adiabatic gradient. Here, $\omega = \kappa\rho\ell_m$ and $\ddot{y}$ is set by the geometry of the convecting bubble. The shape parameter, $\ddot{y}$ is partially what separates the various formulations of MLT. Consistent with the standard DSEP treatment of convection, and LS95, we set $\ddot{y} = 1/3$.

Combining Equations (54)–(58) yields a solution for the convective velocity, which effectively defines the temperature gradient. The entire solution, as with the previous derivations, may be found in its full glory in LS95. For our purposes, we cite yet another set of new variables required to simplify the solution,

$$Q = \delta \tag{59}$$

$$\gamma_0 = \frac{c_P\rho}{2acT^3} \left(\frac{1 + \omega^2/3}{\omega} \right) \tag{60}$$

$$C = \frac{g\ell_m^2 Q}{8H_P} \tag{61}$$

$$V^{-1} = \gamma_0 C^{1/2}.$$
$$\left(\nabla_{rad} - \nabla_{ad} + f\frac{v}{\alpha}\nabla_{ad}\nabla_\chi + (1-f)\frac{v}{\delta}\nabla_\chi \right)^{1/2} \tag{62}$$

$$A = \frac{9}{8} \frac{\omega^2}{(3 + \omega^2)} \tag{63}$$

and, lastly,

$$y = v_{conv} V \gamma_0. \tag{64}$$

Resulting from the combination of the five magnetic MLT equations and the substitution of the variables just defined produces an equation that is quartic in y,

$$\frac{2A}{V} y^4 + y^3 + \left[2A\gamma_0^2 C \left(\frac{\nabla_{ad}}{\alpha} - \frac{1}{Q} \right) (1-f)v\nabla_\chi + 1 \right] Vy^2 -$$
$$y - \frac{C\gamma_0^2 V^3 v}{Q}(1-f)\nabla_\chi = 0. \tag{65}$$

We remark that in the equation above, we deviate from LS95 by the presence of a $1/Q$ in the quadratic term. This difference appears to be the result of the authors accidentally dropping a term in the original derivation. However, as we shall see, this factor will become unimportant.

Finding a solution for y from Equation (65) can easily be obtained numerically. Making an educated guess as to the solution for y we may use a series of Newton–Raphson corrections to converge to a proper solution. A convergence tolerance of 10^{-10} is imposed on the correction term to reduce propagation of large numerical errors. Modifying the original "guess" supplied by LS95 to include the dropped term mentioned above, a good trial solution is

$$y = \left[1 + 2AC\gamma_0^2 v \left(\frac{\nabla_{ad}}{\alpha} - \frac{1}{Q} \right) (1-f)\nabla_\chi \right]^{-1}. \tag{66}$$

One may notice that in the above trial solution (and most other MLT equations), the precise value of the free parameter f has the ability to drastically simplify the expression.

3.4. *The Parameter f and the Frozen Flux Condition*

In Section 3.1 we specified that the plasma under consideration was perfectly conducting and, thus, had zero resistivity. One consequence of assuming an ideal MHD plasma is that magnetic field lines become physical objects that are transported by the plasma, the so-called frozen flux condition (FFC; Alfvén 1942). The magnetic flux is

$$\Phi(t) = \int_{S(t)} \mathbf{B}(\mathbf{r},t) \cdot d\hat{\mathbf{A}}. \tag{67}$$

For an ideal plasma, the evolution of Φ in time is dependent upon not only the time rate of change of the magnetic field, $\mathbf{B}(r, t)$, but also on any distortion occurring to the bounding surface, $S(t)$, as the plasma moves. The net effect is that the time rate of change of the magnetic flux is equal to zero. Therefore, we must have

$$\frac{\partial \mathbf{B}}{\partial t} = 0, \tag{68}$$

which may be rewritten using Equation (1), the induction equation, with $\eta = 0$. This results in the well-known FFC condition,

$$\nabla \times (\mathbf{u} \times \mathbf{B}) = 0. \tag{69}$$

The FFC enforces the restriction that, for a spherically symmetric bubble of plasma undergoing isotropic expansion or contraction (Kulsrud 2004),

$$\frac{B}{\rho^{2/3}} = \text{constant.} \tag{70}$$

Applying this constraint to the magnetic energy gradient definition of a convecting fluid element (Equation (46)), we are able to physically motivate the definition of the parameter f which governs the flux of energy between the fluid element and the surrounding material.

Imagine a region in a star where a small bubble begins to grow convectively unstable. Initially, the bubble has the same properties as the surrounding fluid. It is only because of the change in density that other properties begin changing as well. The FFC allows us to write the magnetic energy contained within a fluid parcel as a function of the magnetic energy of the surrounding material. Since a convecting fluid parcel has a slight under- or overdensity compared to its surroundings, we perturb the element's density

$$\rho_e = \rho_s + \xi \tag{71}$$

where it is understood that $\xi \ll \rho_s$. We also drop the subscript s hereafter. Assuming, for simplicity, that the bubble expands isotropically, the magnetic field strength within a convectively unstable bubble is

$$B_e = \frac{B}{\rho^{2/3}} (\rho + \xi)^{2/3} = B \left(1 + \frac{\xi}{\rho}\right)^{2/3} \tag{72}$$

meaning the magnetic energy per mass may be written as

$$\chi_e = \frac{B_e^2}{8\pi(\rho + \xi)} = \frac{B^2}{8\pi\rho} \left(1 + \frac{\xi}{\rho}\right)^{1/3}. \tag{73}$$

We now have a direct relation between the magnetic energy density of the convecting fluid element and the surrounding material,

$$\chi_e = \chi_s \left(1 + \frac{\xi}{\rho}\right)^{1/3}. \tag{74}$$

Taking the radial, logarithmic derivative,

$$\left(\frac{d\ln\chi}{dr}\right)_e = \left(\frac{d\ln\chi}{dr}\right)_s + \frac{1}{3}\left(\frac{\xi}{\rho+\xi}\right)\left[\frac{d\ln\xi}{dr} - \frac{d\ln\rho}{dr}\right]. \tag{75}$$

The first of the bracketed terms goes to zero, as the density perturbation is independent of radial location. Using the definition of χ_s (Equation (20)) to expand the derivative, and after rearranging the resulting terms, the equation becomes

$$\left(\frac{d\ln\chi}{dr}\right)_e = \frac{d}{dr}\ln\left(\frac{B^2}{8\pi}\right) - \left(\frac{d\ln\rho}{dr}\right)\left[1 + \frac{1}{3}\left(\frac{\xi}{\rho+\xi}\right)\right]. \tag{76}$$

By definition, we know that $\xi/\rho \ll 1$, meaning the perturbation term in the square brackets is negligible. As such,

$$\left(\frac{d\ln\chi}{dr}\right)_e \approx \left(\frac{d\ln\chi}{dr}\right)_s \tag{77}$$

allowing us to conclude that the FFC implies that $f \approx 1$.

3.5. *Magnetic Field Strength Distribution*

The strength of the perturbations described in the preceding sections are determined by the magnitude and spatial gradient of χ. Mentioned in Section 3.3, was that we deviate from the prescription of χ proposed by LS95. Instead of defining

$$\chi = \chi_{\max} \exp\left[-\frac{1}{2}\left(\frac{M_D - M_{Dc}}{\sigma}\right)^2\right], \tag{78}$$

where

$$M_D = \log_{10}\left[1 - \left(\frac{M_r}{M_*}\right)\right], \tag{79}$$

we opt to directly prescribe the radial magnetic field profile. Approaching the problem in this manner, however, introduces the difficulty of selecting a particular radial profile, and without any real confidence of the radial profile inside stars, we are left to our own devices.

One of the simplest profiles to select is that of a dipole configuration, where the field strength drops off as r^{-3} from the magnetic field source location. This is illustrated in Figure 1. The radial profile may then be prescribed as

$$B(R) = B(R_{\text{tach}}) \cdot \begin{cases} (R_{\text{tach}}/R)^3 & R > R_{\text{tach}} \\ (R/R_{\text{tach}})^3 & R < R_{\text{tach}} \end{cases} \tag{80}$$

with the peak magnetic field strength defined to occur at the radius R_{tach}. The radial location described by R_{tach} is the location of the stellar tachocline, an interface between the convective envelope and radiative core. This interface region is thought to be characterized as a strong shear layer where the differentially rotating convection zone meets the radiative core rotating as a solid body. Theory suggests that the tachocline is the source location for the standard mean-field stellar dynamo (i.e., the α–ω dynamo; Parker 1975).

Since DSEP monitors the shell location of the boundary to the convection zone, the tachocline appeared to be a reasonable location, both theoretically and numerically, to base
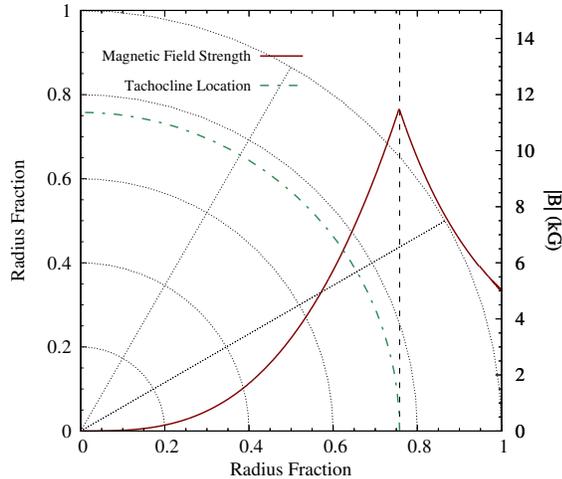
Figure 1. Magnetic field strength profile for a 1.0 $M_\odot$ star with a 5.0 kG photospheric magnetic field strength (maroon, solid). The green dash-dotted line indicates the location of the stellar tachocline, the interface between the radiative and convective regions. The plot is meant only to illustrate the field strength profile. A small gap in the field strength profile is barely perceptible near the surface of the star. This artifact is due to the separation of the stellar interior and envelope integration regimes in the code.

the scaling of the magnetic field strength. However, defining the magnetic field strength at the tachocline ($B(R_{\mathrm{tach}})$) is required. In an effort to allow for direct comparisons between field strengths input into the code and observed magnetic field strengths, the field strength at the tachocline is anchored to the photospheric (surface) magnetic field strength,

$$B(R_{\mathrm{tach}}) = B_{\mathrm{surf}} \left(\frac{R_*}{R_{\mathrm{tach}}} \right)^3 . \qquad (81)$$

where $B_{\mathrm{surf}} = B(R_*)$ is introduced as a new free parameter. The advantage of B_{surf} as a free parameter is that it has potential to be constrained observationally.

Fully convective stars do not possess a tachocline. However, a dynamo mechanism still has the potential to drive strong magnetic fields through an α^2 mechanism (Chabrier & Küker 2006). Full three-dimensional MHD modeling suggests that, in this case, the magnetic field strength peaks at about 0.15 R_* (Browning 2008). Unfortunately, the adopted micro-physics were solar-like and may not be entirely suitable for fully convective M-dwarfs. Regardless of these shortcomings, Browning's investigation provides the only estimate, to date, for the location of the peak magnetic field strength in fully convective stars. As such, we adopt $R_{\mathrm{tach}} = 0.15R_*$ as the dynamo source location in our models of fully convective stars.

3.6. *Numerical Implementation*

Although we have laid out the mathematical construction of the magnetic perturbation, we have yet to illuminate precisely how the perturbation is treated numerically. When a magnetic model is first executed, the user provides a surface magnetic field strength, the geometry parameter γ, and the age at which the magnetic perturbation will occur. The model proceeds to evolve the same as a standard model until the initial perturbation age is reached.

Once the perturbation age is reached, the magnetic field strength profile is prescribed based on the assumed photospheric field strength and the location of the tachocline, as in Figure 1. The magnetic energy and magnetic pressure are then

computed for each of the model's mass shells. Here, the total pressure associated with each mass shell is also perturbed.

Following the introduction of the perturbation, the code must recompute the structure of the stellar envelope, which is separate from the stellar interior integration. The envelope comprises the outer 2%–3%, by radius, of the stellar model. Surface boundary conditions are determined prior to the envelope integration by interpolating within the PHOENIX model atmosphere tables using $\log g$ and T_{eff}. This interpolation returns P_{gas} at the surface of the star, and defines the start of the inward integration. The magnetic perturbation is then explicitly included in the calculation of the analytic EOS.

This leads into the convection routines, where the non-standard stability criterion in Equation (53) is evaluated and judged. Either the equations of magnetic MLT are solved, or the radiative gradient is selected. The envelope integration scheme proceeds until it reaches a pressure commensurate with the pressure for the interior regime.

From the newly calculated envelope, the interior integration begins using a Henyey integration scheme (Henyey et al. 1964) with the magnetic perturbation implemented. The EOS and convection routines are evaluated as in the envelope. Once a final solution is converged upon, the code iterates in time and the process is repeated. For each temporal iteration, the magnetic field profile is adjusted to adapt to changes in the location of the tachocline and changes in the number of mass shells.

4. INITIAL TESTING

In Section 3, we outlined the formulation and implementation of a magnetic perturbation within the framework of DSEP. With the perturbation implemented, it was crucial to perform a series of numerical tests and common-sense checks to validate that the code was operating properly.

The four key numerical tests were to ensure that:

1. The relative change in radius between magnetic models of monotonically increasing photospheric magnetic field strength must also be monotonically increasing with respect to a non-magnetic model.

2. All model adjustments after the initial perturbation must be continuous and smooth.

3. The final perturbed model properties must be independent of the evolutionary stage at which the perturbation is made.

4. The resulting perturbed model must be consistent, regardless of the number of time steps taken after the perturbation.

All of these tests were performed to confirm that the code was producing consistent results and that it was doing so in a numerically stable manner (i.e., no wild fluctuations).

Figure 2 demonstrates that all model adjustments to a magnetic perturbation satisfy each of the four criteria we required for numerical validation. Panel (a) demonstrates that the radius monotonically increases as the surface field strength applied monotonically increases. Changes are observed to be smooth, as seen in panel (b) and are independent of the number (or size) of the evolutionary time steps taken (panel (d)). Finally, the plot in panel (c) indicates that the relative change to the model asymptotes to the same value, regardless of the evolutionary phase at which the perturbation is applied.
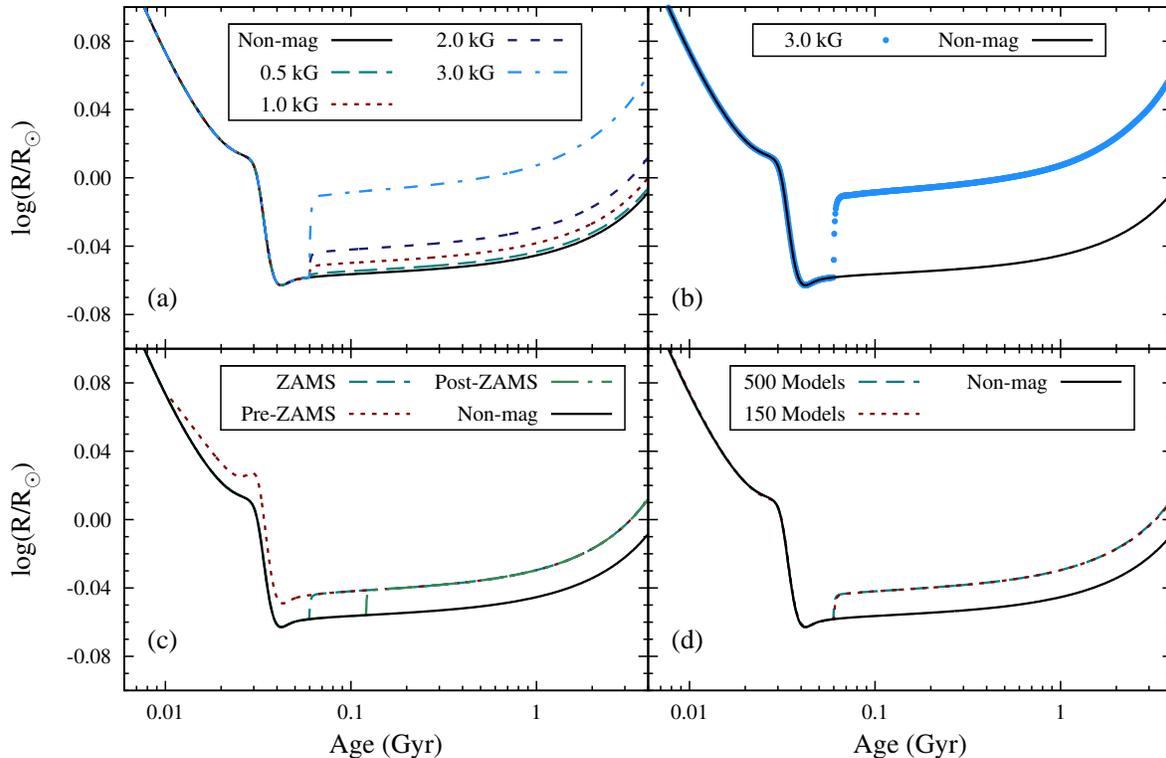
Figure 2. Tests of numerical stability for a 1 $M_\odot$ magnetic model with $\gamma = 2$. (a) Influence of various magnetic field strengths. (b) Evidence of a smooth perturbation at a large magnetic field strength with a relatively large radius change. (c) Consistency among models with the perturbation turned on at various evolutionary stages. (d) Demonstrating the insensitivity of the perturbation to the number of time steps after the perturbation is enabled.

Beyond testing for numerical stability, we must be assured that the code produces results consistent with reality. Typically, a comparison with previous studies would be utilized. However, the only such examples computed for evolutionary timescales are for CM Dra (Chabrier et al. 2007; MacDonald & Mullan 2012). The stellar mass regime occupied by CM Dra would require the implementation of FreeEOS, a task reserved for a future investigation. With the analytical EOS, it would appear there are no models generated with which to compare. Even LS95 operate over timescales on the order of a solar-cycle and not evolutionary times.

In the absence of previous results with which to compare, we opted to impose a weak magnetic field (5 G) on our solar-calibrated model. Seeing as the properties of the Sun do not require a magnetic field in order to produce an adequate solar model (Bahcall et al. 1997), we would expect the solar properties to remain almost entirely unaffected. As expected, the magnetically perturbed model still meets our requirements for it to be considered solar-calibrated (see Section 2). The model radius changes by 3 parts in 10^5 while effective temperature changes by 4 parts in 10^6 given the presence of the weak field.

5. CASE STUDY: EF AQUARII

5.1. *Standard Models*

Standard, non-magnetic mass tracks with solar metallicity were computed for both EF Aqr A and B with masses of 1.24 $M_\odot$ and 0.95 $M_\odot$, respectively. Additional mass tracks were also generated for a scaled-solar metallicity of +0.1 dex. The two components were unable to be fit with a coeval age, regardless of the adopted metallicity. This is consistent with the conclusions of Vos et al. (2012). Two fitting methods were performed to this end.

We first attempted to fit both components on an age–radius

plane, which is equivalent to fitting on the mass–radius (M–R) plane. This is illustrated by the solid lines in Figure 3(a). The primary star evolves much more rapidly than secondary, owing to the rather large mass difference. Thus, the model radius of the primary inflates to the observed radius at an age of 2.0 Gyr. The radius of the primary then quickly exceeds the observational bounds within about 0.1 Gyr. The observational bounds on the primary radius places tight constraints on the allowed age our models predict for the system. However, our model of the secondary does not reach the observed radius until an age of 6.3 Gyr, an age difference of 4.3 Gyr between the two components. This 4.3 Gyr difference is consistently present in our models, including when mass and composition are allowed to vary within the observed limits (not shown).

Assuming the age of the system was predicted accurately using models of EF Aqr A in the M–R diagram, we find that the model radius of EF Aqr B underpredicts the observed radius by 11%. Again, consistent with the findings of Vos et al. (2012), who found a radius discrepancy of 9%. Such a disagreement is also broadly consistent with results from other studies of active EBs (Ribas 2006; Torres et al. 2010).

A second approach was to fit the system on an HR diagram using the individual mass tracks. Figure 3(b) demonstrates that the standard model tracks do not match the observed $T_{\rm eff}$–luminosity of either star, despite fitting the stars individually in the M–R plane. Our models predict temperatures that are 250 K (4%) and 430 K (8%) hotter than the observations for the primary and secondary, respectively.

The noticeable temperature disagreements in both stars may be the result of two possible effects. On the one hand, we might assume that the age predicted from the M–R plane is correct and that there only exists a discrepancy with the effective temperatures. This implies that either the effective
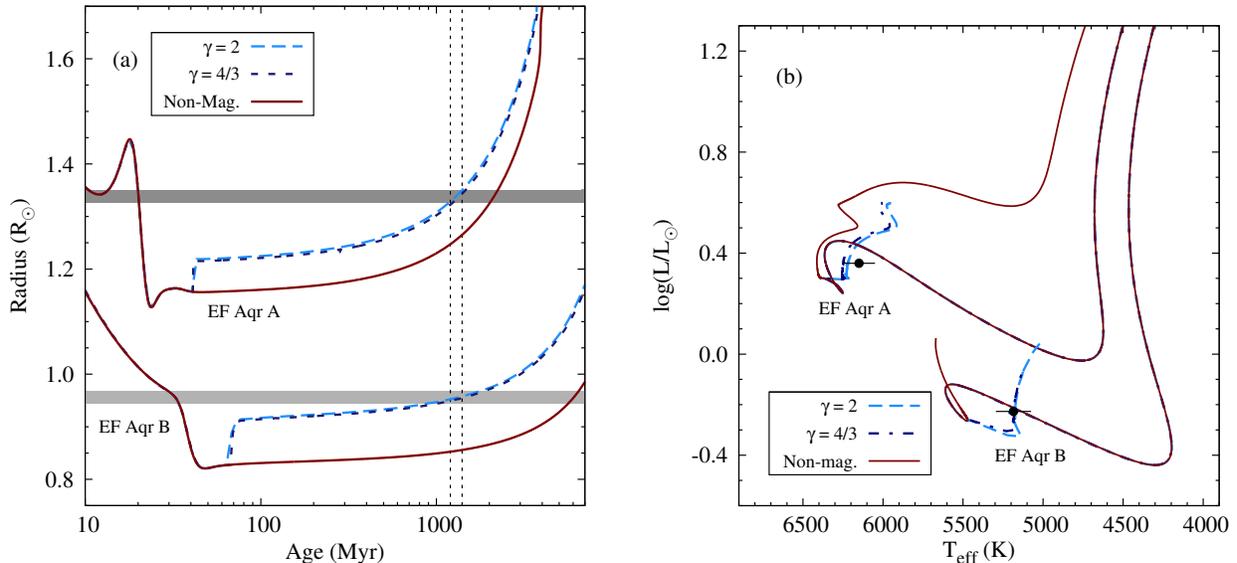
Figure 3. Individual stellar mass tracks representing EF Aqr A and B (labeled). Non-magnetic mass tracks are shown as a red, solid line while $\gamma = 2$ and $\gamma = 4/3$ magnetic tracks are indicated by the blue, long-dash and light-blue, short-dash lines, respectively. The corresponding photospheric magnetic field strengths for EF Aqr A are 1.6 kG ($\gamma = 2$) and 2.6 kG ($\gamma = 4/3$). For EF Aqr B they are 3.2 kG ($\gamma = 2$) and 5.5 kG ($\gamma = 4/3$). (a) Age–radius diagram with the observed radii marked as gray regions. Vertical dotted lines define the age constraint imposed by EF Aqr A, suggesting the system has an age of 1.3 ± 0.2 Gyr. (b) HR diagram with the observed data marked as black points.

temperature from the models or the observations is incorrect. However, since the stars are quite similar to the Sun, it is more likely the case that our standard models underpredict the radius of the primary as well, driving up the model-derived effective temperature. This particular scenario is supported by Vos et al. (2012) who found both components display obvious Ca II emission that is likely the result of each star having a magnetically heated chromosphere.

The age inferred from the M–R diagram would then be older than the true age of the system. Unfortunately, this scenario further complicates the situation regarding EF Aqr B. If the age of the system is younger than inferred from standard models of the primary, then the radius discrepancy for the secondary becomes larger than originally quoted.

5.2. Magnetic Models

Following the results discussed above, magnetic models were computed for both EF Aqr components using a scaled-solar heavy element composition. Several models with a mass of 1.24 $M_\odot$ were generated with various surface magnetic field strengths. We then found the model with the weakest field strength required to produce the observed radius and T_{eff} of EF Aqr A. With $\gamma = 2$, we had to prescribe a photospheric magnetic field strength of 1.6 kG, while with $\gamma = 4/3$, a more intense 2.6 kG field was necessary. The magnetic model tracks are displayed in Figures 3(a) and (b) as blue dashed lines. The magnetic models of the primary suggest a younger age of 1.3 ± 0.2 Gyr for the EF Aqr system, as opposed to the 2.0 Gyr age determined from standard models. This younger age is consistent with the 1.5 ± 0.2 Gyr age derived for the primary by Vos et al. (2012) after fine-tuning the mixing length.

We next had to select a magnetic field strength that would allow a 0.95 $M_\odot$ model to have a radius and T_{eff} compatible with EF Aqr B at 1.3 Gyr, if finding that unique combination was possible. Surface magnetic field strengths of 3.2 kG and 5.5 kG were able to produce the required stellar parameters, with $\gamma = 2$ and 4/3, respectively, at an age of 1.35 Gyr. In both cases, the models were able to reproduce the stellar radius and T_{eff} within the quoted 1σ uncertainties. Figures 3(a) and (b)

demonstrate that the magnetic models do indeed match both component radii and T_{eff}s at a common age.

Structurally, the addition of a magnetic perturbation within the models reduces the radial extent of the surface convection zone. For both stars in EF Aqr, we find the magnetic models that are sufficient to correct the observed discrepancies have surface convection zones that are 4% smaller than those in the standard models, at the same age. The reduction of the surface convection zone can be attributed to the modified stability criterion as well as modified convective velocities. While only speculation, we attribute the equality of the percent reduction of convection zone sizes to coincidence.

6. DISCUSSION

6.1. Field Strengths

The implementation of a magnetic perturbation within stellar evolution models is quite capable of reconciling predicted model fundamental stellar properties with those determined observationally, at least for EF Aqr. While it seems plausible that magnetic fields may suppress thermal convection inside solar-type stars, how are we to be sure that magnetic fields may be reasonably invoked for this particular system? Even if invoking magnetic fields is rational, are the field strengths required by the models realistic?

Addressing the first question, we showed in Section 1 that naturally inefficient convection, as described by the Bonaca et al. (2012) calibration, was unable to account for the small values of α_{MLT} required to mitigate the observed model-observation disagreements. But, the inability of naturally inefficient convection to provide a solution does not positively identify magnetic fields as the root cause. However, there is additional evidence that invoking magnetic fields is reasonable.

High-resolution spectroscopy of the Ca II H and K lines for both stars in EF Aqr reveals incredibly strong emission cores superposed on the absorption troughs (Vos et al. 2012). A search of the *ROSAT* Bright Source Catalogue (Voges et al. 1999) also shows that EF Aqr is a strong X-ray emitter. Coupling these observations with high projected rotational veloc-

ities extracted from line broadening measurements, suggests that there is the potential for a strong dynamo mechanism to be operating. This evidence is only circumstantial, but does provide tantalizing clues.

For the sake of argument, let us assume that the stars are significantly magnetically active. It would then be worthwhile to compare the strength of the magnetic field for each EF Aqr component to those values required by the models. Unfortunately, no direct magnetic field strength estimates of EF Aqr are available, forcing us to base our analysis on indirect magnetic field strength estimates.

A natural first step would be to compare the EF Aqr components to other known solar-type stars, such as the Sun and α Cen A and B (see Table 2). The Sun's mean photospheric magnetic field strength is between 0.1 G and 1 G (Babcock & Babcock 1955; Babcock 1959; Demidov et al. 2002) with local patches of very intense fields (i.e., sunspots) with strengths on the order of 2–3 kG (Hale 1908). Similarly, the average longitudinal field strength of α Cen A was determined to be less than 0.2 G, after a null detection of a Stokes *V* polarization signature (Kochukhov et al. 2011).

The field strengths required by the models of the EF Aqr components therefore suggest that the stars are pervaded by magnetic fields that typically characterize the intense regions of sunspots. This at first appears detrimental to the validity of the models. However, studies of the active and quiet Sun, particularly sunspot regions, has led to multiple scaling relations allowing for an indirect determination of stellar photospheric magnetic field strengths.

One of these scaling relations was observed to exist between the X-ray luminosity of an active region and its total unsigned magnetic flux (Fisher et al. 1998; Pevtsov et al. 2003). The two observables were found to exhibit a power-law relation,

$$L_x \propto \Phi^p, \tag{82}$$

where the power-law index, p, was determined to be 1.19±0.04 by Fisher et al. (1998). The index was later revised by Pevtsov et al. (2003) using a more diverse data set, including both solar and extrasolar sources.[7] Their revised analysis decreased the index to $p = 1.15$. The magnetic flux is defined in the usual manner (Equation (67)),

$$\Phi = \int_S \mathbf{B} \cdot d\hat{\mathbf{A}} = \int_S |B_z| \, dA. \tag{83}$$

with $|B_z|$ represents the vertical magnetic field strength. Therefore, if we are able to determine the X-ray luminosity of the EF Aqr components, it is possible to place a lower limit on the magnetic field strength at the surface of the two components.

The system has a confirmed X-ray counter-part in the *ROSAT* All-Sky Survey Bright Source Catalogue (Voges et al. 1999). The X-ray count rate was converted to an X-ray flux according to the formula derived by Schmitt et al. (1995),

$$F_x = (5.30\text{HR} + 8.31) \times 10^{-12} X_{\text{cr}}, \tag{84}$$

where HR is the X-ray hardness ratio,[8] X_{cr} is the X-ray count rate, and F_x is the X-ray flux. Finally, the X-ray flux was

converted to a luminosity using the 172 pc distance quoted by Vos et al. (2012).

The count rate measured by *ROSAT* was 0.0655±0.0154 counts s^{-1} with a hardness ratio of 0.32±0.22. This yields an X-ray flux of 6.55×10^{-13} erg cm^{-2}. Weighting the contribution of each star to the total X-ray flux is reliably performed in one of two ways: by assuming both stars contribute equally (valid if for binaries if stars are similar in radius; Fleming et al. 1989) or weighting proportional to $v_{rot} \sin i$ (Pallavicini et al. 1981; Fleming et al. 1989). Given the similarity of the two stars in EF Aqr, the precise weighting does not affect the results. If both stars contribute equally to the total X-ray flux, then at a distance of 172 pc, the X-ray luminosity of each component is $L_x = 1.16 \times 10^{30}$ erg s^{-1}. Alternatively, weighting the two stars based on their projected rotational velocity gives $L_{x,A} = 1.25 \times 10^{30}$ erg s^{-1} and $L_{x,B} = 1.07 \times 10^{30}$ erg s^{-1}.

To provide a comparison, the X-ray luminosity of a typical solar active region is on the order of 10^{27} erg s^{-1} (Fisher et al. 1998; Pevtsov et al. 2003). The Sun, on average, has a total X-ray luminosity of 10^{27} erg s^{-1} up to nearly 10^{28} erg s^{-1}, depending on where in its activity cycle it is located (Ayers 2009). Similarly, Ayers (2009) monitored the X-ray luminosity of α Cen and found the primary had an X-ray luminosity around half that of the Sun (approximately 10^{27} erg s^{-1}) and the secondary had about twice the X-ray luminosity of the Sun (about 10^{28} erg s^{-1}). Further estimates for the X-ray luminosity of α Cen A and B comes from *ROSAT*, which yields luminosities between 10^{27} erg s^{-1} and 10^{28} erg s^{-1} for each component, consistent with Ayers' analysis. Table 2 provides a comparison of how these quantities translate to magnetic field strengths.

Comparisons with the Sun and α Cen show that each component in EF Aqr has an X-ray luminosity 2–3 orders of magnitude greater than "typical" G and early-K stars. Again, while not indicative of causation, the correlation between high levels of X-ray emission and magnetic activity strongly suggests that EF Aqr is incredibly active. Given this information, our initial assumption that the stars are active seems valid. Therefore, the implementation of a magnetic perturbation in stellar models of this system appears warranted.

The amount of vertical magnetic flux near the surface of each star may then be found using the Pevtsov et al. (2003) scaling relation. This suggests $\Phi = 1.39 \times 10^{26}$ Mx associated with each component (given equal flux contribution). Converting to a magnetic field strength involves dividing the unsigned magnetic flux by the total area through which the field is penetrating. For our purposes, the area is the entire surface area of the star. Therefore, we find the vertical magnetic field strength for the primary and secondary of EF Aqr to be 1.3 kG and 2.5 kG, regardless of the adopted flux weighting, respectively. Note, this is the vertical magnetic field strength and sets a lower limit to the total magnetic field strength. It should also be mentioned that the X-ray luminosities calculated for EF Aqr A and B are near the edge of the data sample utilized by Pevtsov et al., although no extrapolation of the relation was required.

Further estimates of the magnetic field strengths may be found by applying a scaling relation using the Ca II K line core emission (Schrijver et al. 1989). The scaling relation was developed by correlating Ca II K line core emission and the magnetic flux density of solar active regions and their sur-

---

[7] The total unsigned magnetic flux of the stellar sources was obtained using direct observational techniques (Saar 1996).

[8] There are typically two hardness ratios listed in the *ROSAT* catalog, HR1 and HR2. The Schmitt et al. (1995) formula requires the use of HR1.

Table 2
Estimated Magnetic Field Strengths (in G)

Star	Direct	X-Ray	Ca II	DSEP
Sun	0.1 - 1.0	5 - 20	⋯	⋯
α Cen A	< 0.2	∼3	⋯	⋯
α Cen B	⋯	∼49	⋯	⋯
EF Aqr A	⋯	1300	830	1600 - 2600
EF Aqr B	⋯	2500	3300	3200 - 5500

roundings. The relation between the two was found to be

$$\frac{I_c - 0.13}{I_w} = 0.008\langle Bf\rangle^{0.6} \quad (85)$$

where I_c is the intensity of the emission line core, I_w is the intensity of the line wing. While the relation was derived for small, local active regions, Schrijver et al. (1989) suggest that there is no reason to believe that the relation would not hold for hemispherical averages of solar-type stars.

Using the spectra provided by Vos et al. (2012) for the Ca II K core emission lines from each EF Aqr component, we were able to estimate the magnetic field strength of each component. Spectra for the primary indicate that the average magnetic field strength, $\langle Bf\rangle$, is equal to 830 G. Similarly, for EF Aqr B, $\langle Bf\rangle = 3.3$ kG. The values quoted above are derived from rough approximations of the core and wing intensities. However, we do not foresee the values of $\langle Bf\rangle$ changing radically with more precise line intensity measurements. We do caution that the results for EF Aqr B require an extrapolation of the Ca II relation and the data for EF Aqr A place it near the edge of the derived relation where only a few data points exist.

Based on the scaling relations for X-ray emission and Ca II K line core emission, the magnetic field strength for the primary and secondary is seen to be approximately 1 kG and 3 kG, respectively. The magnetic field strengths required by the models are therefore within a factor of two of the predicted field strengths, regardless of the adopted γ value. Since we expect the X-ray emission prediction to be a lower limit to the full magnetic field strength, this is extremely encouraging. The models do not require abnormally large field strengths to reconcile the model properties with those from observations, particularly when a γ value of 2 is adopted.

6.2. Implications

The introduction of self-consistent magnetic stellar evolution models has multiple applications, ranging from studies of exoplanet host stars (Torres 2007; Charbonneau et al. 2009; Muirhead et al. 2012) to investigations of cataclysmic variable (CV) donor stars (Knigge et al. 2011), as well as to studies attempting to probe the stellar initial mass function of young clusters, where stars are typically very magnetically active (Johns-Krull 2007; Jackson et al. 2009; Yang & Johns-Krull 2011). Although, most obvious, are the implications for studies of low-mass eclipsing binary systems (see, e.g., Torres et al. 2010; Parsons et al. 2012, and references therein). Low-mass stellar evolution models have been highly criticized for being unable to predict the radii and effective temperatures of DEB stars. Models incorporating magnetic effects open the door to probing the underlying cause of the model-observation disagreements and providing semi-empirical corrections to models.

Magnetic fields have long been theorized as the culprit, but previous generations of models have only treated magnetic fields in an ad hoc manner. Comparing the results of these methods with the one presented in this work, both in terms of surface parameters and the underlying interior structure, will provide an interesting test of their validity. Ultimately, the ad hoc models disagree on the dominant physical mechanism underlying the observed discrepancies. The availability of self-consistent magnetic models should help to settle the debate as to which mechanism (suppressed convection or starspots) is most at work.

For EF Aqr, the models suggest that magnetic suppression of thermal convection is sufficient to reconcile the models with the observations. Since stars with small convective envelopes, such as those discussed in this work, are more sensitive to adjustments of the convective properties, it is not wholly surprising that suppressing convection is sufficient to explain the observations. Whether this mechanism will be adequate for stars near the fully convective boundary has yet to be seen. Future work modeling the lowest-mass DEB systems will clarify this ambiguity. Regardless, this may suggest why the largest radius deviations are predominantly observed at higher masses (Feiden & Chaboyer 2012), with the notable exception of CM Dra (Terrien et al. 2012).

The nature of our models allows for independent verification of the magnetic field strengths required as input. While the indirect estimates provided by X-ray emission and Ca II K emission are encouraging, confirmation of these results using high resolution Zeeman spectroscopy, spectropolarimetry, or Zeeman–Doppler imaging (ZDI) is preferred. Unfortunately, these observations are difficult for fast rotators, such as those that comprise most DEB systems. They are also difficult for distant systems, where the short integration time required by ZDI inhibits the ability of acquiring measurements with sufficient signal-to-noise (see the reviews by Donati & Landstreet 2009; Reiners 2012). Once a magnetic field is detected, there exists the question of whether the observed strength is indicative of the total magnetic field strength. Field strengths derived for stars with spectral-type K and M using Stokes V observations appear to yield only around 10% of the total magnetic field strength compared to observations in Stokes I (Reiners & Basri 2009). This is a consequence of the fact that regions of opposite polarity tend to cancel out in Stokes V, making it most sensitive to the large-scale component, not the small-scale fields thought to pervade low-mass stars. How to accurately account for this when testing the models is not fully clear and will require investigation. As more stars across all spectral types are observed in both Stokes V and I, a more coherent picture is sure to develop.

Magnetic models may also be useful for transiting exoplanet surveys, particularly those focused on M-dwarfs (e.g., MEarth transit survey; Nutzman & Charbonneau 2008; Irwin et al. 2009). One of the largest uncertainties in deriving the properties of a transiting planet is the radius of the host star. The lack of reliability involved in predicting low-mass stellar radii from evolution models has deterred the use of models as predictors of exoplanet host-star radii (Torres 2007; Charbonneau et al. 2009). Shoring up these deficiencies may lead to more accurate predictions of host star radii from stellar models, circumventing, for a time, the need for lengthy and costly observations. This would be most useful in identifying interesting follow-up targets by providing a better estimate of the habitable zone (Muirhead et al. 2012).

There are certainly caveats with models, as other large uncertainties exist in predicting the properties of a single star

from stellar evolution mass tracks (Basu et al. 2012). However, work is being performed to alleviate some of these uncertainties by calibrating models to asteroseismic data (Bonaca et al. 2012). Low-mass stars are also less sensitive to the input parameters of stellar models than their solar-type counterparts, reducing the associated uncertainties. Stellar evolution models may therefore provide a fast and reliable estimate of the host star properties, depending on the required level of precision.

Since most M-dwarfs being surveyed are nearby, there is a good chance that they may have an X-ray counterpart in either the Bright Source or Faint Source Catalogue from the *ROSAT* All-Sky Survey (Voges et al. 1999, 2000). As was demonstrated in Section 6.1, magnetic field strengths required by the models are within about a factor of two (or better, if $\gamma = 2$ is adopted) of those predicted by the X-ray scaling relation of Pevtsov et al. (2003). This will allow an intelligent choice of the magnetic field strength used as an input for the models, thus producing more reliable results from stellar models.

All told, the introduction of a self-consistent set of magnetic stellar evolution models provides the potential for models to be used with greater reliability in a wide range of applications. There still exist several challenges that require attention (Boyajian et al. 2012), but this is a first step in addressing key issues that have been raised in the past two decades.

REFERENCES

Alfvén, H. 1942, Nature, 150, 405
Ayers, T. R. 2009, ApJ, 696, 1931
Babcock, H. W. 1959, ApJ, 130, 364
Babcock, H. W. & Babcock, H. D. 1955, ApJ, 121, 349
Bahcall, J. N., Basu, S., Pinsonneault, M., & Serenelli, A. M. 2005, ApJ, 618, 1049
Bahcall, J. N., Pinsonneault, M., Basu, S., & Christensen-Dalsgaard, J. 1997, Physical Review Letters, 78, 171
Baraffe, I., Chabrier, G., Allard, F., & Hauschildt, P. H. 1998, A&A, 337, 403
Barnes, S. A. 2010, ApJ, 722, 222
Basu, S., Verner, G. A., Chaplin, W. J., & Elsworth, Y. 2012, ApJ, 746, 76
Bender, C. F., Mahadevan, S., Deshpande, R., et al. 2012, ApJ, 751, L31
Berger, D. H., Gies, D. R., McAlister, H. A., et al. 2006, ApJ, 644, 475
Bjork, S. R. & Chaboyer, B. 2006, ApJ, 641, 1102
Böhm-Vitense, E. 1958, Z. Astrophys., 46, 108
Bonaca, A., Tanner, J. D., Basu, S., et al. 2012, ApJ, 755, L12
Boyajian, T. S., von Braun, K., van Belle, G., et al. 2012, ApJ, 757, 112
Browning, M. 2008, ApJ, 676, 1262
Carter, J. A., Fabrycky, D. C., Ragozzine, D., et al. 2011, Science, 331, 562
Chaboyer, B., Fenton, W. H., Nelan, J. E., Patnaude, D. J., & Simon F. E. 2001, ApJ, 562, 521
Chaboyer, B. & Kim, Y.-C. 1995, ApJ, 454, 767
Chabrier, G. & Baraffe, I. 1997, A&A, 327, 1039
Chabrier, G., Gallardo, J., & Baraffe, I. 2007, A&A, 472, L17
Chabrier, G. & Küker, M. 2006, A&A, 446, 1027
Charbonneau, D., Berta, Z. K., Irwin, J., et al. 2009, Nature, 462, 891

Demarque, P., Woo, J-H., Kim, Y.-C., & Yi, S. K. 2004, ApJS, 155, 667
Demidov, M. L., Zhigalov, V. V., Peshcherov, V. S., & Grigoryev, V. M. 2002, Sol. Phys., 209, 217
Donati, J. F. & Landstreet, J. D. 2009, ARA&A, 47, 333
Dotter, A., Chaboyer, B., Jevremović, D., et al. 2007, AJ, 134, 376
Dotter, A., Chaboyer, B., Jevremović, D., et al. 2008, ApJS, 178, 89
Doyle, L. R., Carter, J. A., Fabrycky, D. C., et al. 2011, Science, 333, 1602
Feiden, G. A. & Chaboyer, B. 2012, ApJ, 757, 42
Feiden, G. A., Chaboyer, B., & Dotter, A. 2011, ApJ, 740, L25
Ferguson, J. W., Alexander, D. R., Allard, F., et al. 2005. ApJ, 623, 585
Fisher, G. H., Longcope, D. W., Metcalf, T. R., & Pevtsov, A. A. 1998, ApJ, 508, 885
Fleming, T. A., Gioia, I. M., & Maccacaro, T. 1989, ApJ, 340, 1011
Gough, D. O. & Tayler, R. J. 1966, MNRAS, 133, 85
Grevesse, N., & Suaval, A. J. 1998, Space Sci. Rev., 85, 161
Guenther, D. B., Demarque, P., Kim, Y.-C., & Pinsonneault, M. H. 1992, ApJ, 387, 372
Gurnett, D. A. & Bhattacharjee, A. 2005, Introduction to Plasma Physics (Cambridge: Cambridge Univ. Press)
Hale, G. E. 1908, ApJ, 28, 315
Hauschildt, P. H., Allard, F., & Baron, E. 1999a, ApJ, 512, 377
Hauschildt, P. H., Allard, F., Ferguson, J., Baron, E., & Alexander, D. R. 1999b, ApJ, 525, 871
Henyey, L. G., Forbes, J. E., & Gould, N. L. 1964, ApJ, 139, 306
Iglesias, C. A. & Rogers, F. J., 1996, ApJ, 464, 943
Irwin, J., Charbonneau, D., Nutzman, P., & Falco, E. 2009, in IAU Symp. 253, Transiting Planets, ed. F. Pont, D. Sasselov, & M. Holman (Cambridge: Cambridge Univ. Press), 37
Irwin, J. M., Quinn, S. N., Berta, Z. K., et al. 2011, ApJ, 742, 123
Jackson, J. D. 1998, Classical Electrodynamics (3rd ed.; Hoboken, NJ: Wiley)
Jackson, R. J., Jeffries, R. D., & Maxted P. F. L. 2009, MNRAS, 399, L89
Johns-Krull, C. M. 2007, ApJ, 664, 975
Knigge, C., Baraffe, I., & Patterson, J. 2011, ApJS, 194, 28
Kochukhov, O., Makaganiuk, V., Piskunov, N., et al. 2011, ApJ, 732, L19
Kraus, A. L., Tucker, R. A., Thompson, M. I., Craine, E. R., & Hillenbrand, L. A. 2011, ApJ, 728, 48
Kulsrud, R. M. 2004, Plasma Physics for Astrophysics (Princeton, NJ: Princeton Univ. Press)
Lacy, C. H. 1977, ApJ, 218, 444
López-Morales, M. 2007, ApJ, 660, 732
Lydon, T. J. & Sofia, S. 1995, ApJS, 101, 357
MacDonald, J. & Mullan, D. J., 2012, MNRAS, 421, 3084
Mathis, S. & Zahn, J.-P 2005, A&A, 440, 653
Morales, J. C., Gallardo, J. J., Ribas, I., et al. 2010, ApJ, 718, 502
Morales, J. C., Ribas, I., & Jordi, C. 2008, A&A, 478, 507
Morales, J. C., Ribas, I., Jordi, C., et al. 2009, ApJ, 691, 1400
Muirhead, P. S., Hamren, K., Schlawin, E., et al. 2012, ApJ, 750, L37
Mullan, D. J. & MacDonald, J. 2001, ApJ, 559, 353
Nutzman, P., & Charbonneau, D. 2008, PASP, 120, 317
Pallavicini, R., Golub, L., Rosner, R., et al. 1981, ApJ, 248, 279
Parker, E. N. 1975, ApJ, 198, 205
Parsons, S. G., Marsh, T. R., Gänsicke, B. T., et al. 2012, MNRAS, 420, 3281
Pevtsov, A. A., Fisher, G. H., Acton, L. W., et al. 2003, ApJ, 598, 1387
Popper, D. M. 1997, AJ, 114, 1195
Reiners, A. 2012, Living Rev. Solar Phys., 9, 1
Reiners, A. & Basri, G. 2009, A&A, 496, 787
Ribas, I. 2006, Ap&SS, 304, 89
Richard, O., Michaud, G., & Richer, J. 2005, ApJ, 619, 538
Saar, S. H. 1996, in IAU Colloq. 153: Magnetodynamic Phenomena in the Solar Atmosphere, Prototypes of Stellar Magnetic Activity, ed. Y. Uchida, T. Kosugi, & H. S. Hudson (Dordrecht: Kluwer), 367
Schmitt, J. H. M. M., Fleming, T. A., & Giampapa, M. S. 1995, ApJ, 450, 392
Schrijver, C. J., Coté, J., Zwaan, C., & Saar, S. H. 1989, ApJ, 337, 964
Skumanich, A. 1972, ApJ, 171, 565
Skumanich, A., Smythe, C., & Frazier, E. N. 1975, ApJ, 200, 747
Spada, F. & Demarque, P. 2012, MNRAS, 422, 2255
Stassun, K. G, Kratter, K. M., Scholz, A., & Dupuy, T. J. 2012, ApJ, 756, 47
Terrien, R. C., Fleming, S. W., Mahadevan, S., et al. 2012, ApJ, 760, L9
Thoul, A. A., Bahcall, J. N., & Loeb, A. 1994, ApJ, 421, 828
Torres, G. 2007, ApJ, 671, L65
Torres, G., Andersen, J., & Giménez, A. 2010, A&AR, 18, 67
Torres, G. & Ribas, I. 2002, ApJ, 567, 1140
Vitense, E. 1953, ZAp, 32, 135
Voges, W., Aschenbach, B., Boller, Th., et al. 1999, A&A, 349, 389

Voges, W., Aschenbach, B., Boller, Th., et al. 2000, VizieR Online Data Catalog, 9029, 0

Vos, J., Clausen, J. V., Jørgensen, U. G., et al. 2012, A&A, 540, 64

Winn, J. N., Albrecht, S., Johnson, J. A., et al. 2011, ApJ, 741, L1

Yang, H. & Johns-Krull, C. M. 2011, ApJ, 729, 83